J Mater Sci (2010) 45:2958–2966
DOI 10.1007/s10853-010-4292-z

Synthesis and characterization of bimodal rod-like mesoporous carbons from raffinose by SBA-15 templates

Xiufang Wang · Yong Tian · Guosheng Song · Linquan Zang

Received: 14 August 2009 / Accepted: 1 February 2010 / Published online: 17 February 2010

Abstract Mesoporous carbons with bimodal rod-like pore structures and tunable pore sizes from 3.66 to 5.42 nm were for the first time obtained by employing SBA-15 as templates and raffinose as carbon precursors. Small angle X-ray diffraction, transmission electron microscopy, scanning electron microscopy, N_2 sorption analysis, and Raman spectroscopy were used to determine the textural properties of the resulting materials. Bimodal frameworks with mesopores (4–5 nm) as well as macropores (125–130 nm) were achieved. The mesoporous carbons lost its ordered structure from the templates due to mesostructural shrinkage and collapse of mesopores, which resulted in partial duplicate of the template and pore-widening effect (meso to macropores). With the increasing of carbonization temperature from 500, 700 to 900 °C, the textural parameters such as specific surface areas, pore volumes, and mean pore diameters all increased significantly. In the temperature range studied, higher carbonization temperature would generate much more abundant porosity. The ratio of I_D to I_G (I_D/I_G) indicated a rather low crystallinity with the varying of aging temperature and the carbonization temperatures. The advantage of the procedure was that no acid or other chemical catalysts were involved during the infiltration and carbon formation process.

X. Wang · Y. Tian (✉) · L. Zang
College of Pharmacy, Guangdong Pharmaceutical University, Guangzhou Higher Education Mega Center, Guangzhou 510006, China
e-mail: fengshoutian@hotmail.com

G. Song
Analytical and Testing Center, South China University of Technology, Guangzhou 510640, China

Introduction

Mesoporous materials, due to their remarkable properties such as high specific surface area, narrow pore-size distribution, tunable pore structure, large pore volume, and high thermal and mechanical stability, have attracted great technological interest for the development of purification of water, electronic, catalytic, and energy storage systems [1–8]. Moreover, the excellent biocompatibility and controllable pore-size distributions make them highly prospective and valuable in drug delivery systems [9]. In recent years, researches on mesoporous materials with potential applications in the field of biomedicine have increased significantly. Because these materials demonstrated the capability to load and release large amounts of drugs, an important evolution has been carried out on the basis of their promising characteristics as drug delivery systems [9, 10] In this sense, different chemical surface functionalizes for a more efficient charge and delivery of drugs [11], proteins [12], and even DNA [13] have been studied. However, for specific applications such as drug delivery system, it is very difficult to achieve mesoporous carbons with strictly controlled pore structures due to the complexity of the carbon structure evolution and the selective regulation of pore structures still remains unresolved.

The synthesis of ordered mesoporous carbon (OMC) was first reported [14] in 1999 by a nanocasting route using ordered mesoporous silica (MCM-48) as the hard template. In parallel to nanocasting, various OMC materials have been synthesized, based on the high variety of mesoporous silica structures, which are usually synthesized through the cooperative assembly of inorganic precursors and amphiphilic surfactants, involving either a hydrothermal or an evaporation-induced self-assembly (EISA) pathway [15, 16]. Furthermore, great efforts have been taken to

widen the range of materials accessible via self-assembly technique. Among the various synthetic methods of OMCs [17–23], the solid template method, which involves the impregnation with a carbon precursor followed by pyrolysis and template removal, is widely used and remains a powerful tool for the creation of nanostructured materials because it allows control of structures and morphology of the resulting products, despite that it is associated with some disadvantages, such as the need to prepare the hard template (porous silica) and the template removal process.

Studies concerning furfuryl alcohol [17, 18] and sucrose [24, 25] as carbon sources had been carried out. Raffinose was a kind of trisaccharide that had been widely used. As far as we know, mesoporous materials with bimodal pore structures from raffinose have never been reported in the literature. The advantage of the procedure was that no acid or other chemical catalysts were involved during the infiltration and carbon formation process. In this contribution, a series of mesoporous carbons with bimodal rod-like frameworks were for the first time obtained by employing SBA-15 as templates and raffinose as carbon precursors. The influence of aging temperature of the templates and the carbonization temperature were investigated. It is aimed that the materials synthesized by this strategy can find their further application in drug delivery systems.

Experimental

Synthesis procedure

Synthesis of SBA-15 templates

According to the method previously reported by Zhao [3] and Dai [6], P123 (poly(ethylene oxide) poly(propylene oxide) poly (ethylene oxide) triblock copolymer) (PEO20-PPO70-PEO20; Aldrich) was used as the structural directing agent and TEOS (Tetraethyl orthosilicate, Fuchen Chemical Regent of Tianjin) was used as the silica source. In a typical synthesis, 8.00 g of P123 was added to 288 mL of a 1.7 M aqueous solution of hydrochloric acid and the mixture was stirred for 4 h at 40 °C. Next, 8.00 g of TEOS was added dropwise and the polymer was continuously stirred for 3 h. The resulting gels were transferred to the Teflon-lined sealed containers and were kept at 70, 100, and 130 °C for 48 h under static hydrothermal conditions. Then the products were filtered, washed with water, and dried for 12 h at 80 °C. The as-synthesized samples were divided into two portions. One portion (~1 g) was extracted with a mixture of 200 mL of EtOH 95% (v/v) and 4 mL of concentrated HCl at 60–70 °C in a Soxhlet extractor for 24 h twice. After a second stage of drying at 80 °C for 24 h, the samples were collected and denoted as SBA-15-70, SBA-15-100, and SBA-15-130. The other portion (~1 g) was carbonized at 550 °C for 4 h under flowing air and a heating rate of 5 °C/min. The samples obtained by carbonization were labeled as SBA-15-70#, SBA-15-100#, and SBA-15-130#. All chemicals were used as received without further purification. Ultra pure water was used in all experiments.

Synthesis of mesoporous carbons

Raffinose was utilized as the carbon precursor and SBA-15 was used as the template. An ethanol/water (v/v, 1:1) solution of raffinose with the concentration of 0.15 g/mL was prepared. Typically, 1.0 g of SBA-15-70 was infiltrated with 5.0 mL of raffinose solution (0.15 g/mL, aforementioned), and magnetically stirred continuously until ethanol was completely evaporated (about 30 min). The paste was cured at 80 °C for 6 h and then at 150 °C for 6 h for the solidification of raffinose inside the pores of SBA-15-70. The above impregnation step was repeated for another time to ensure that the pores were filled with raffinose. The as-synthesized sample was pyrolyzed at 900 °C (3 °C/min) under flowing N_2 atmosphere (200 mL/min) for 3 h. The composite was washed with HF solution (20%) for the removal of silica template, followed by washing with abundant water until the pH value was close to 7. The products were dried at 80 °C for 24 h. It should be noted that the usage of raffinose was calculated according to the pore volume of the SBA-15 templates. Typically, the calculated usages of raffinose solution (0.15 g/mL) were 9.8, 17.5, 6, 10.4, and 10.6 mL, respectively, for SBA-15-100, SBA-15-130, SBA-15-70#, SBA-15-100#, and SBA-15-130#. The carbonized products were labeled as C–*X*–*Y* or C–*X*–*Y*#, where *X* refers to the aging temperature of the template, *Y* refers to the carbonization temperature of the final carbon products, and # refers to the carbonization of the templates. For example, C-70-900 refers to products carbonized at 900 °C by the template SBA-15-70. C-70-900# refers to products carbonized at 900 °C by the template SBA-15-70#.

Characterization

Characterizations were taken by powder X-ray diffraction, nitrogen adsorption at -196 °C, transmission electron microscopy (TEM), scanning electromagnetic microscopy (SEM), and Raman spectroscopy. The small angle XRD patterns were recorded on a Multi Purpose Diffractometer (PANanalytical. Inc. X'Pert Pro., MPD) with Cu KR radiation (0.1540 nm), using an operating voltage of 40 kV and 40 mA, 0.017° step size, and 4.96 s step time. Microscope glass slides were used as sample supports. The

samples were manually ground prior to the XRD analysis and all measurements were performed at room temperature. Nitrogen adsorption isotherms were measured with Micromeritics Tristar 3020 volumetric adsorption analyzers at 77 K. Before adsorption measurements, samples were degassed under vacuum at 200 °C for 4 h. The specific surface area of the samples was calculated by using the BET method. The pore-size distributions were derived from the adsorption branches of isotherms by using the Barett–Joyner–Halenda (BJH) model, and the total pore volumes (V_t) were estimated from the adsorbed amount at a relative pressure p/p_0 of 0.99. TEM experiments were conducted on a JEOL 2011 microscope operated at 200 kV. The samples for TEM measurements were suspended in ethanol and supported onto a holey carbon film on a Cu grid. Raman spectroscopy measurements were made on a HORIBA Jobin–Yvon LabRAM Aramics with a microscope attachment, using a He–Ne laser with a wavelength of 633 nm. FTIR measurements were carried out on Vector 33(Bruker) for the analysis for full template removal.

Results

The XRD patterns of the SBA-15 templates and the carbonized samples with different templates were shown in Fig. 1. Pore structures as well as the unit cell parameter "a" and the wall thicknesses were calculated as shown in Table 1. The nitrogen sorption isotherms and the corresponding pore-size distributions for the templates SBA-15 were shown in Fig. 2. Figure 3 showed the parameters of the carbonized products and Fig. 4 showed the textural properties of the pyrolyzed materials by varying carbonization temperature with the same templates SBA-15-100 and SBA-15-100#. Figure 5 showed the SEM and TEM images of the carbonized products as a sample. The influence of aging temperature of the templates and the carbonization temperature were investigated.

Discussion

Textural properties

Figure 1 showed the XRD patterns of the SBA-15 templates and the carbonized samples with different templates. Basically, all the samples showed three well-resolved XRD peaks with 100,110, and 200 reflections of the 2D hexagonal symmetry, indicating a good structural quality of these materials and the patterns can be assigned to an ordered structure of hexagonal symmetry with p6mm space group. The most intense reflection is the (100) peak and the d100 spacing were calculated to be 8.99–10.94 nm (Table 1).

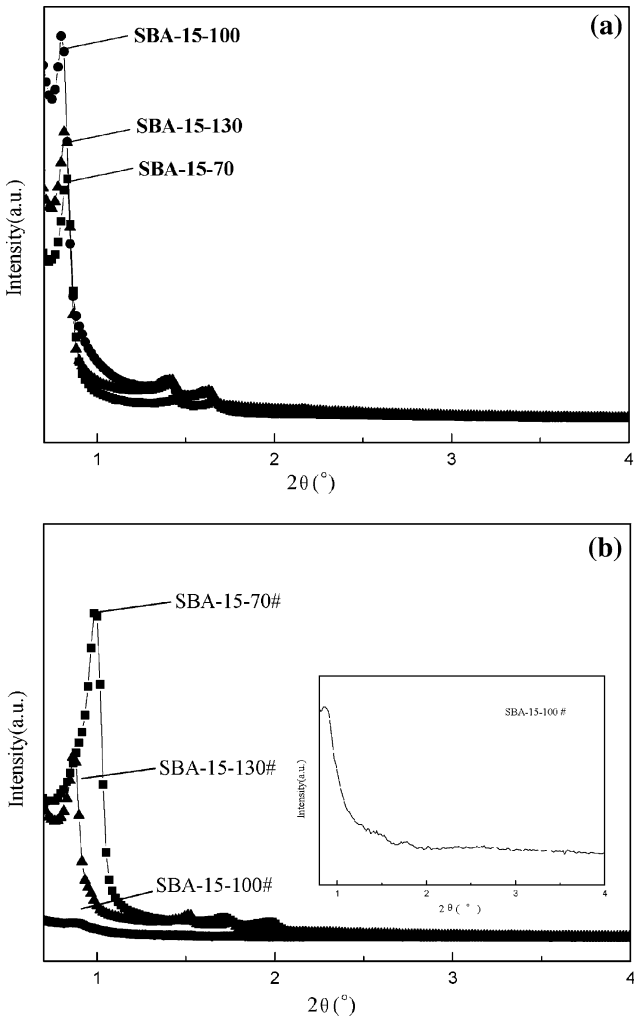

Fig. 1 Small angle XRD patterns for SBA-15 templates (the *inset* figure in **b** is the enlarged diffraction curve of SBA-15-100#)

The unit cell parameter "a" and the wall thicknesses were calculated as shown in Table 1.

The nitrogen sorption isotherms for the templates SBA-15 (Fig. 2a, c) exhibit type IV curves with an obvious capillary condensation at a relative pressure $P/P_0 =$ 0.6–0.8 and a H_1-type hysteresis loop, indicating a uniform structure of the mesopores. The corresponding pore-size distributions (Fig. 2b, d) are very narrow, centering at ~7 nm with big wall thicknesses. Whereas, the nitrogen sorption isotherms for the resulting pyrolyzed materials (Fig. 3a, c) showed type IIb curves with an obvious capillary condensation at a relative pressure $P/P_0 =$ 0.5–0.8 as well as multi-layer adsorption ($P/P_0 =$ 0.9–1.0), indicating the ununiformity of structures. Bimodal mesoporous carbons with the existing of mesopores (4–5 nm) as well as macropores (120–125 nm) were proved by the pore-size distribution curves (Fig. 3b, d). The rod-like frameworks were further proved by the SEM and TEM images (Fig. 4).

Table 1 The textural parameters for SBA-15 templates and for the carbonized products

Textural parameters for SBA-15 templates						
Sample	S_{BET} (m^2/g)	V_t (cm^3/g)	D_{pore} (nm)	a (nm)	d-spacing (nm)	Wall thickness (nm)
SBA-15-70	898	1.04	6.57	12.27	10.63	5.70
SBA-15-100	587	0.97	7.67	12.63	10.94	4.96
SBA-15-130	1175	1.79	7.66	14.21	12.31	6.55
SBA-15-70#	453	0.60	6.74	10.38	8.99	3.64
SBA-15-100#	702	1.06	7.78	14.02	12.14	6.24
SBA-15-130#	692	1.07	7.76	11.76	10.18	4.00

Textural parameters for the carbonized products							
Sample	S_{BET} (m^2/g)	V_t (cm^3/g)	D_{pore} (nm)	Sample	S_{BET} (m^2/g)	V_t (cm^3/g)	D_{pore} (nm)
C-70-900	1349	0.92	3.66	C-70-900#	1356	1.31	4.46
C-100-900	1206	1.05	4.36	C-100-900#	1338	1.45	5.02
C-130-900	1208	1.08	4.33	C-130-900#	1179	1.39	5.43
C-100-500	792	0.58	3.82	C-100-500#	775	0.59	4.08
C-100-700	1098	0.97	4.26	C-100-700#	1298	1.32	4.71
C-100-900	1206	1.05	4.36	C-100-900#	1338	1.45	5.02

S_{BET} specific surface area calculated within the relative pressures of 0.05–0.2, V_t single-point pore volume corresponding to the amount adsorbed at the relative pressure of 0.99, D_{pore} pore sizes derived from the adsorption branches of isotherms by using the Barett–Joyner–Halenda (BJH) model, *a* unit cell parameter calculated for the most intense reflection peak on each small angle XRD pattern, *d*-spacing (100) interplanar spacing for the most intense reflection peaks

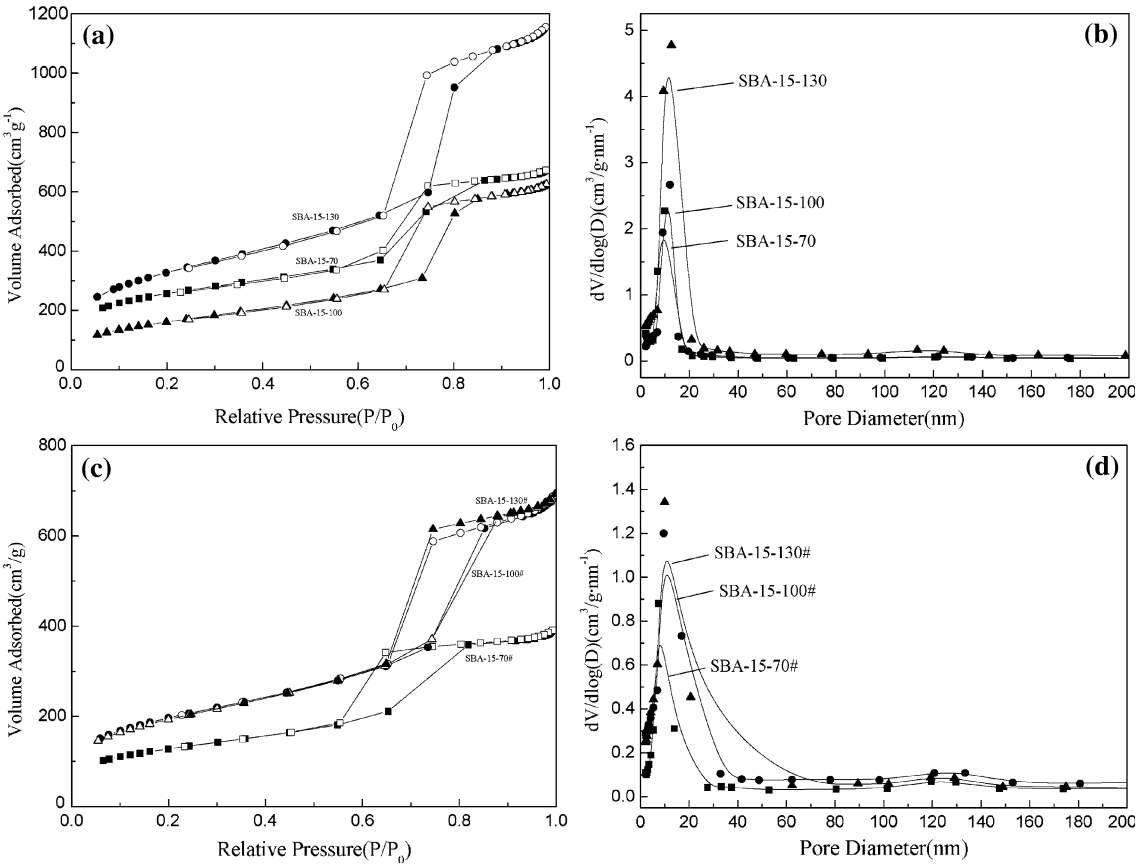

Fig. 2 N_2 sorption isotherms (**a**, **c**) and pore-size distributions (**b**, **d**) for SBA-15 templates

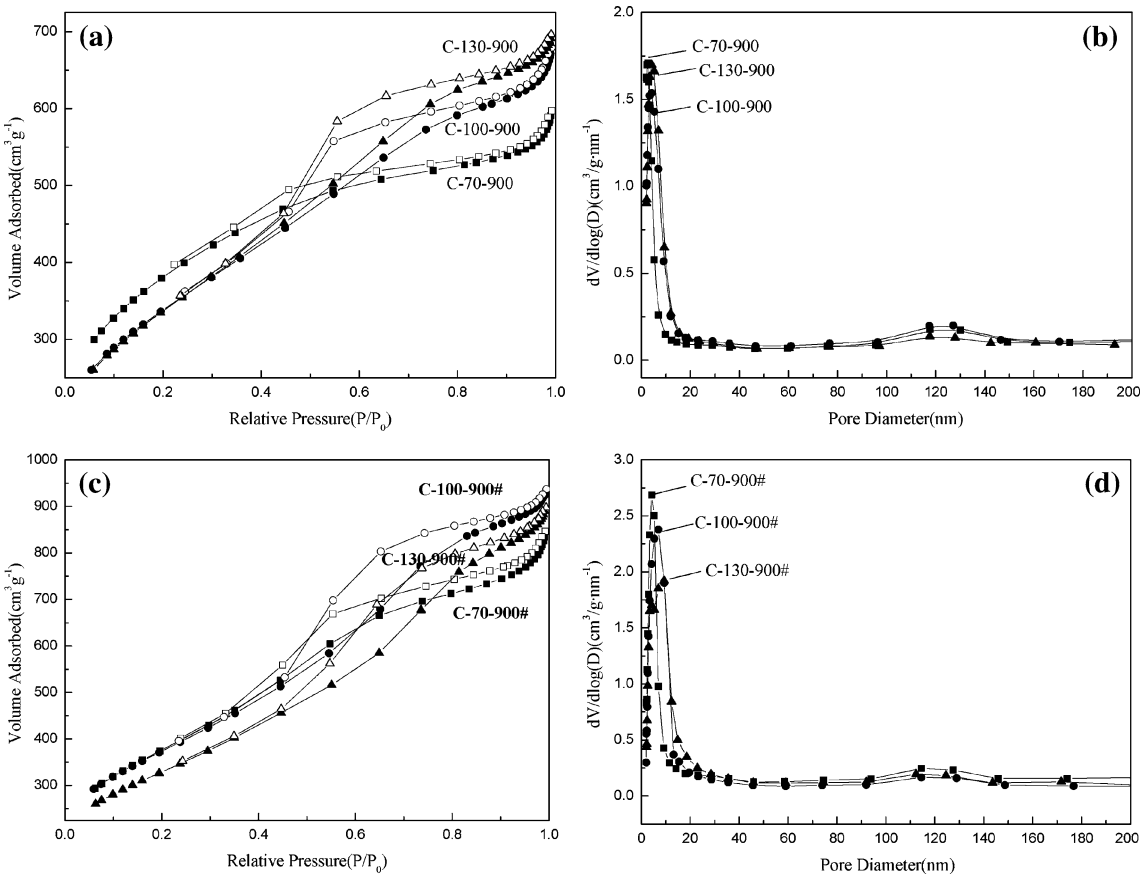

Fig. 3 N_2 sorption isotherms (**a**, **c**) and pore-size distributions (**b**, **d**) for the carbonized products using different SBA-15 templates

From the textural parameters listed in Table 1, one can see that the SBA-15 templates synthesized by solvent extraction had very similar textural properties with those by carbonization steps. The calculation based on the isotherms showed that the SBA-15 templates were characterized by a high BET surface areas, large pore volume, and a narrow pore-size distribution for solvent extraction(SBA-15), and for carbonization steps (SBA-15#). As a contrast, the textural parameters for the carbonized products by the solidification of raffinose inside the pores of SBA-15 templates all inclined to produce approximately higher BET surface areas (1200–1300 m^2/g) and smaller mean pore diameters (4–5 nm) than the templates. Compared with C-900, C-900# had larger pore volumes. Interestingly, bimodal pore-size distributions were noticeable. Unfortunately, the mesopores carbons totally lost its ordered structure from the templates. The absence of spatial order in obtained carbon samples we think may be due to impossibility of generation of cross-linked carbon framework without mineral acid (which catalyzes dehydration, oligomeryzation's processes), that is why carbon structure undergoes to collapse after template dissolution. Moreover, mesostructural shrinkage and collapse of mesopores would result in the partial duplicate of the template and pore-widening effect (mesopores to macropores). These results were in agreement with what had been previously reported by Roggenbuck and Tiemann [26] and Lu et al. [27]. Moreover, there might be another possibility. The appearance of macropores can also be explained by sorption and following pyrolysis processes on external surface of silica particles due to large size of raffinose molecules (comparatively with mono- and di-saccharides) and using of some surplus of carbon precursor.

Effect of temperature on structure and porosity

Compared with SBA-15-70# and SBA-15-130#, the (100) diffraction for SBA-15-100# was less intense, indicating the less ordered structure of the template. The enlarged XRD diffraction peak of SBA-15-100# (inset figure of Fig. 1b) showed a small angle diffraction at $2\theta = 0.88°$. The pore sizes and the wall thicknesses for the SBA-15 templates varied with aging temperature of hydrothermal treatment. At the same time, one can see that the XRD peak of SBA-15-100 was more intense than those of SBA-15-70 and SBA-15-130, showing that aging temperature of

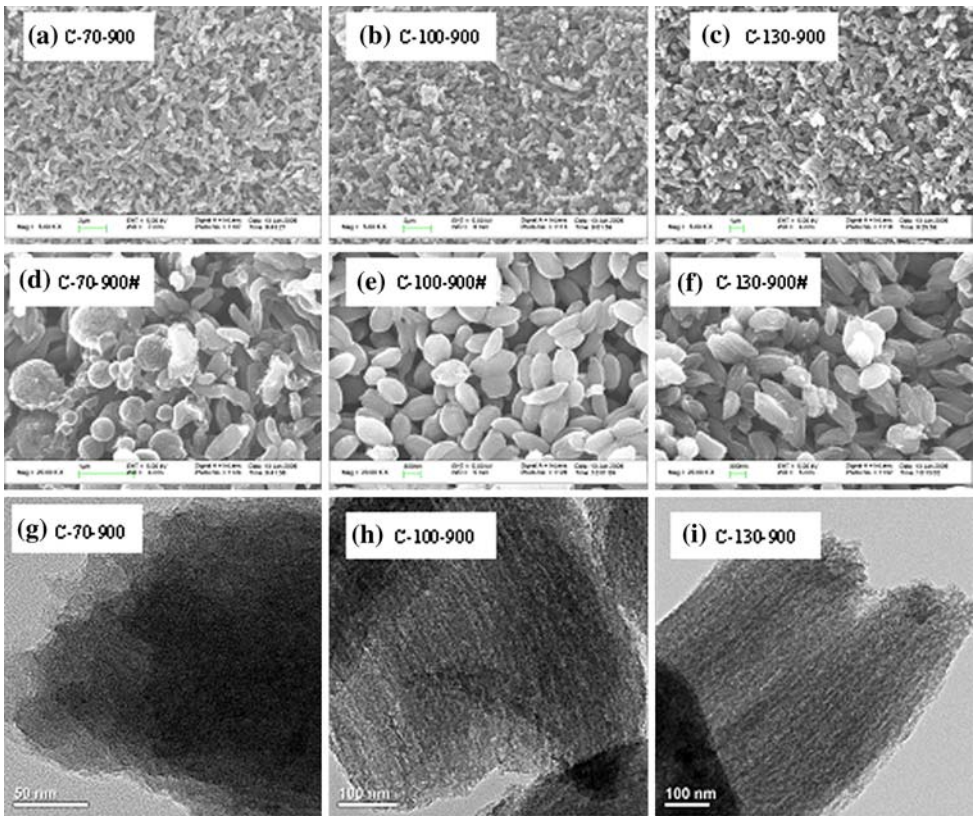

Fig. 4 The SEM and TEM images of the pyrolyzed mesoporous materials after template removal

hydrothermal treatment had great influence on the ordered property of the final products. Higher aging temperature at 130 °C would result in a less intense of the XRD reflection peak, which may be due to the hydrothermal instability of the materials. It is noticeable that the structural parameters from the solvent extraction of P123 template were slightly larger than those by carbonization steps.

As for the pyrolyzed materials by varying carbonization temperature with the same templates SBA-15-100 and SBA-15-100# as shown in Fig. 5 and Table 1, clearly, the carbonization temperature had great influence on the textural properties of the resulting mesoporous materials. With the increasing of temperature from 500, 700 to 900 °C, the textural parameters such as BET surface areas, pore volumes, and mean pore diameters all increased significantly. Furthermore, the bimodal structures were more visible for C–*X*–*Y* than for C–*X*–*Y*#. In the temperature range studied, higher carbonization temperature would generate much more abundant porosity. As seen in Table 1, sample C-100-900 and C-100-900# showed the highest specific surface area, pore volume, and mean pore diameter for C-100-900, being slightly smaller than for C-100-900#. Due to the combined effects from the structural shrinkage and further developed porosity by the thermal decomposition of the carbon framework, a sharp increase of the textural parameters was observed from C-100-500 to C-100-700, but only very small increase was embodied from C-100-700 to C-100-900. The same trend was determined for C-100-500#, C-100-700#, and C-100-900#.

Figure 4a–f vividly showed the SEM images of the products. Rod-like frameworks were observed, which clearly gave the evidence for the presence of mesopores along with a small amount of macropores. For the SBA-15# templates by carbonization steps, the carbon frameworks inclined to somewhat spherical as shown in Fig. 4d, e, f. The TEM images were given in Fig. 4g–i as a sample, which further proved the textural properties of the materials with abundant mesopores along with a small amount of macropores but almost disordered frameworks. The estimated mesopore diameters were also identical with the results of N_2 sorption analysis as listed in Table 1. At the same time, the pore-widening effect due to the mesostructural shrinkage and collapse of mesopores were also in agreement with the above results of N_2 sorption analysis. The disordered structure of the products was also proved by the XRD analysis (Fig. 6a) as an example. Figure 6b showed the nitrogen adsorption/desorption isotherms of the carbon material obtained by direct carbonization of raffinose (without SBA-15) at 900 °C for 3 h. As compared with Fig. 3 and Fig. 5, different isotherm types were detected and nitrogen adsorption only occurs on the external surface, which suggested that direct carbonization of raffinose with no SBA-15 template would not result in mesoporous structure and even no pores inside.

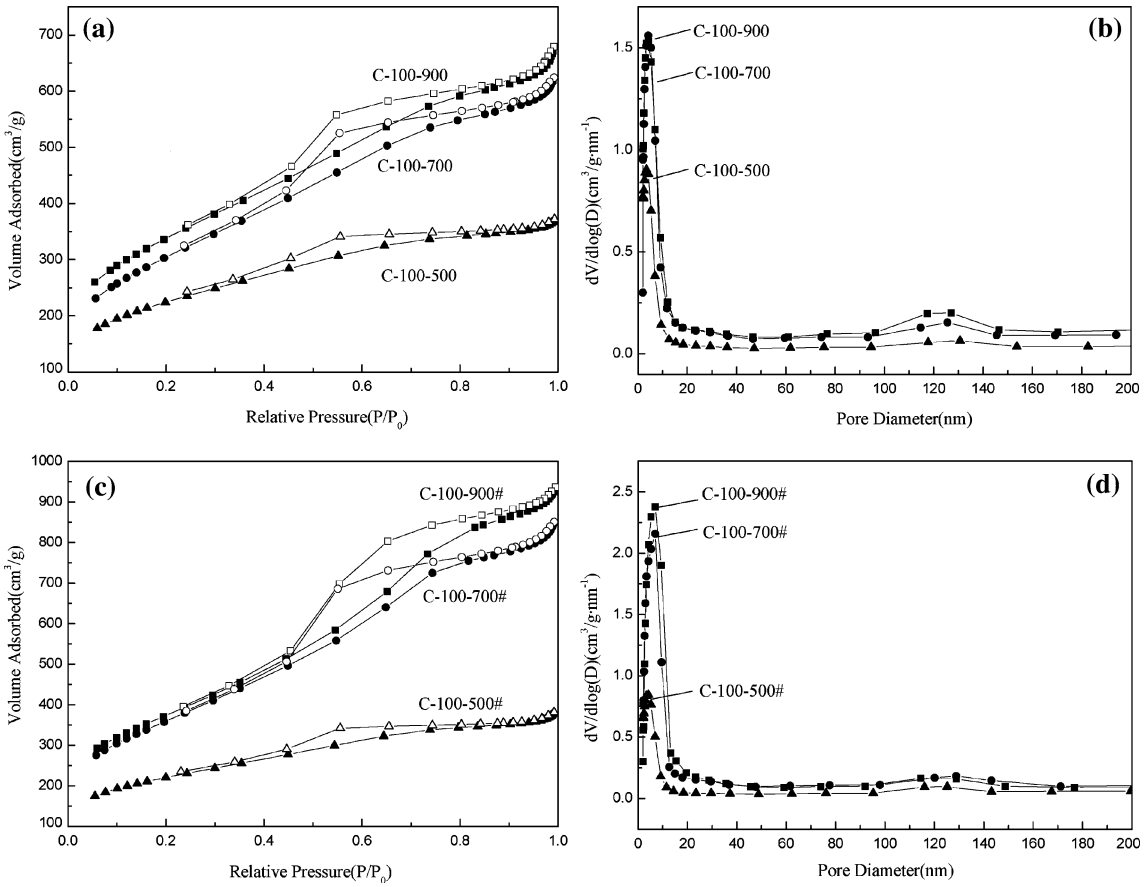

Fig. 5 Nitrogen sorption isotherms (**a**, **c**) and the corresponding pore-size distributions (**b**, **d**) for the pyrolyzed products at different carbonization temperatures

Raman spectroscopy is extensively used for the characterization of carbons [24, 25]. The Raman spectra of pyrolyzed composites (after template removal by HF) were shown in Fig. 7. Two distinct broad bands at a wave number of about 1322 cm^{-1} (D band) and 1599 cm^{-1} (G band) were observed. The D bands indicated the defects and disorders of graphitic materials, whereas, the G bands were assigned to the in-plane displacement of the carbon atoms in hexagonal carbon sheets. A strong D band as shown in Fig. 7 denoted the presence of abundant disordered carbons in the mesoporous materials. Figure 7a demonstrated that the intensity of D bands (I_D) and G bands (I_G) of the pyrolyzed samples increased with the increasing of the aging temperature and was stronger for those from SBA-15# templates than for those from SBA-15 templates. As for the products by varying the carbonization temperature from SBA-15 templates (Fig. 7b) and from SBA-15# templates (Fig. 7c), the intensity was varying, depending on the thermal treatment temperatures. C-100-500 had the lowest intensity and C-100-700 had the highest intensity, with C-100-900 having moderate intensity. Whereas, C-100-500# had the highest intensity and C-100-700# had the lowest intensity, with C-100-900# having moderate intensity. Similar results were obtained with the ratio of I_D to I_G (I_D/I_G) and FWHM (Full Wave at Half Maximum), implying a rather low crystallinity with the varying of the aging temperature and the carbonization temperatures. These results for disordered mesoporous materials were consistent with the findings from N_2 sorption results and XRD analysis, but contrary to the results for ordered mesoporous materials as reported by Garrone et al. [24, 25]. The advantage of the procedure was that no acid or other chemical catalysts were involved during the infiltration and carbon formation process.

To determine whether the silica template was totally removed during extraction, FTIR measurements were carried out and the results of template SBA-15-70 and C-70-900 were shown in Fig. 8 as an example. The transmittance for the template SBA-15-70 at 464 and 1082 cm^{-1} was the stretching vibration of Si–O–Si group and the transmittance at 958 cm^{-1} was the stretching vibration of Si–OH group. Whereas, the transmittance for C-70-900 showed no corresponding vibration, which indicated that silica template was fully removed.

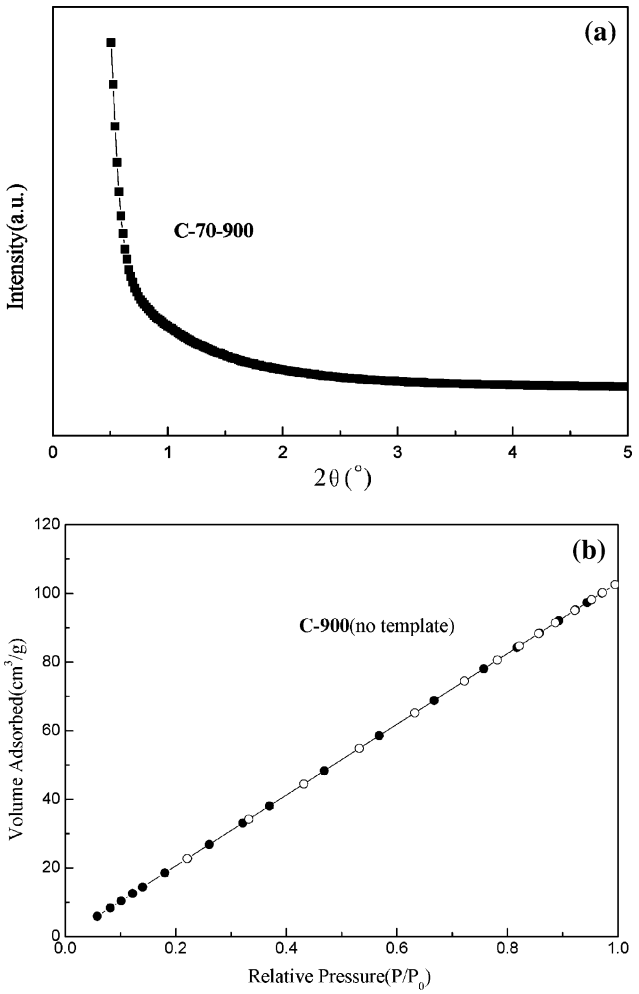

Fig. 6 Small angle XRD pattern for the product carbonized at 900 °C with SBA-15-70 template (**a**) and without SBA-15 template (**b**)

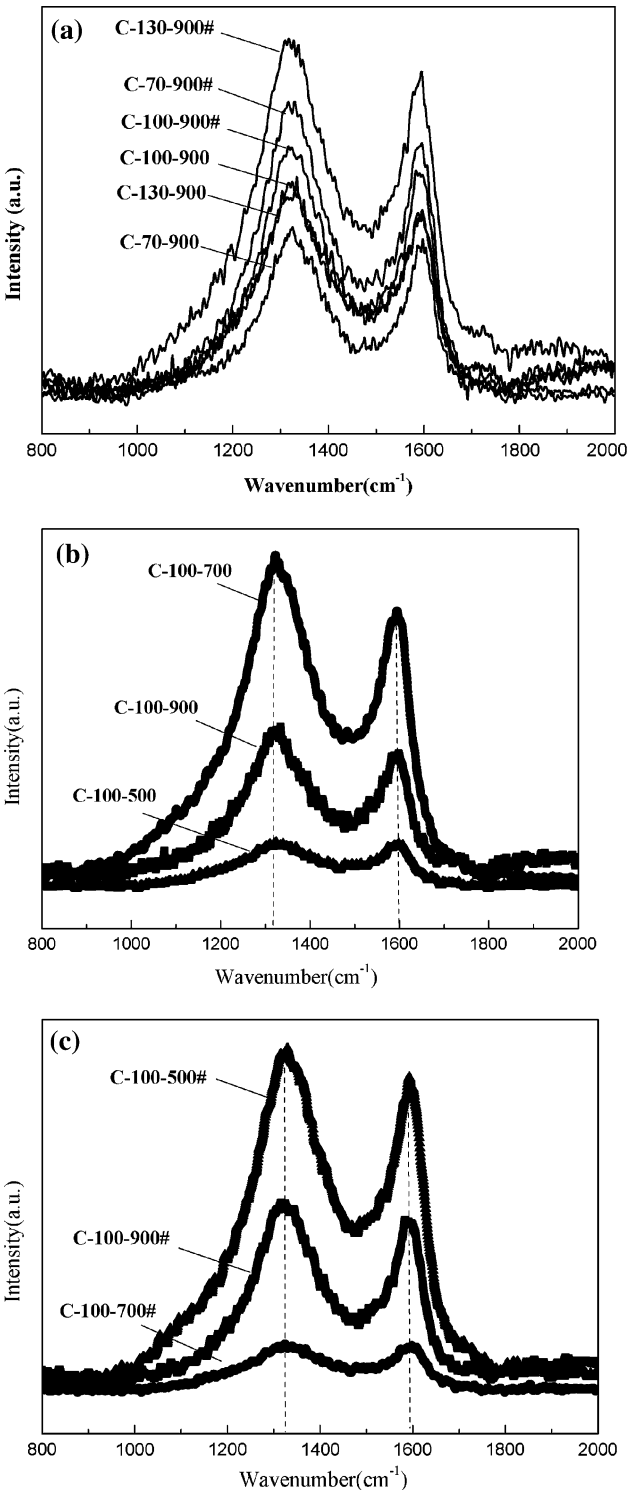

Fig. 7 Raman spectra for the pyrolyzed mesoporous materials after silica template removal

Conclusions

Bimodal rod-like pore structures of mesoporous carbons with tunable pore sizes from 3.66 to 5.42 nm were synthesized by using hard template cast approach (SBA-15 as templates and raffinose as carbon precursors). The advantage of the procedure was that no acid or other chemical catalysts were involved during the infiltration and carbon formation process. Bimodal frameworks with the presence of mesopores (4–5 nm) as well as macropores (125–130 nm) were achieved. The resulting mesoporous materials totally lost its ordered structure from the templates due to mesostructural shrinkage and collapse of mesopores, which resulted in the partial duplicate of the template and pore-widening effect (meso to macropores). The textural parameters such as BET surface areas, pore volumes, and mean pore diameters all increased significantly with the increasing of carbonization temperature from 500, 700 to 900 °C. In the temperature range studied, higher carbonization temperature would generate much more abundant porosity. Furthermore, the bimodal structures were more visible for C–*X*–*Y* than for C–*X*–*Y*#. The ratio of I_D to I_G (I_D/I_G) indicated a rather low crystallinity with the

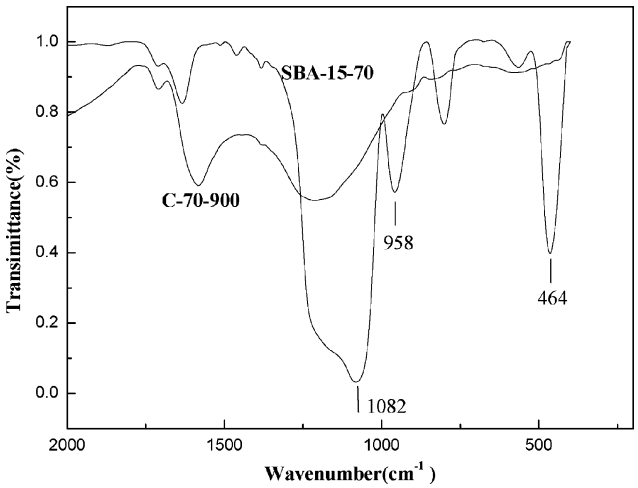

Fig. 8 FTIR spectra for SBA-15-70 and C-70-900

varying of the aging temperature and the carbonization temperatures. It is aimed that the materials synthesized herein can find their further application in drug delivery systems.

Acknowledgements The authors acknowledge the financial support from the National Science Foundation of China (No.50802017), the Medical Science Research Fund of GuangDong Province (No.B2009118) and the Teaching Staff Construction Fund of Guangdong Pharmaceutical University.

References

1. Li XT, Chen XH, Song HH (2009) J Mater Sci 44:4661. doi: 10.1007/s10853-009-3714-2
2. Inomata K, Otake Y (2009) J Mater Sci 44:4200. doi: 10.1007/s10853-009-3560-2
3. Yang HF, Yan Y, Liu Y, Zhang FQ, Zhang RY, Meng Y et al (2004) J Phys Chem B 108:17320
4. Shin Y, Fryxell GE (2008) Chem Mater 20:981
5. Lu AH, Spliethoff B, Schuth F (2008) Chem Mater 20:5314
6. Fulvio PF, Jaroniec M, Liang CD, Dai S (2008) J Phys Chem C 112:13126
7. Liu YR (2009) J Mater Sci 44:3600. doi:10.1007/s10853-009-3487-7
8. Mirzaeian M, Hall PJ (2009) J Mater Sci 44:2705. doi: 10.1007/s10853-009-3355-5
9. Arcos D, Lopez-Noriega A, Ruiz-Hernandez E, Terasaki O, Vallet-Regi M (2009) Chem Mater 21(6):1000
10. Vallet-Regi M, Balas F, Arcos D (2007) Angew Chem Int Ed 46:7548
11. Balas F, Manzano M, Horcajada P, Vallet-Regi M (2006) J Am Chem Soc 128:8116
12. Slowing II, Trewyn BG, Lin VSY (2007) J Am Chem Soc 129:8845
13. Torney F, Trewyn BG, Lin VSY, Wang K (2007) Nat Nanotechnol 2:295
14. Ryoo R, Joo SH, Jun S (1999) J Phys Chem B 103:7743
15. Ying JY, Mehnert C, Wong MS (1999) Angew Chem Int Ed 38(1):56
16. Lu AH, Schuth F (2006) Adv Mater 18:1793
17. Lu AH, Schmidt W, Spliethoff B, Schuth F (2003) Adv Mater 15(19):1602
18. Kim TW, Park IS, Ryoo R (2003) Angew Chem 115:4511
19. Lee HI, Kim JH, You DJ, Lee JE, Kim JM, Ahn WS et al (2008) Adv Mater 20:757
20. Vinu A (2008) Adv Funct Mater 18:816
21. Jiang XG, Brinker CJ (2006) J Am Chem Soc 128:3451
22. Yuan SL, Zhang XQ, Chan KY (2009) Langmuir 25:2034
23. Kadib AE, Hesemann P, Molvinger K, Brandner J, Biolley C, Gaveau P et al (2009) J Am Chem Soc 131:2882
24. Armandi M, Bonelli B, Otero Arean C, Garrone E (2008) Microporous Mesoporous Mater 112:411
25. Armandi M, Bonelli B, Karaindrou EI, Otero Arean C, Garrone E (2008) Catal Today 138:244
26. Roggenbuck J, Tiemann M (2005) J Am Chem Soc 127:1096
27. Lu AH, Schmidt W, Spliethoff B, Schuth F (2004) Chem Eur J 10:6085